

## NEUROSYSTEMS

# Auditory and visual interactions between the superior and inferior colliculi in the ferret

Iain Stitt, Edgar Galindo-Leon, Florian Pieper, Karl J. Hollensteiner, Gerhard Engler and Andreas K. Engel  
Department of Neurophysiology and Pathophysiology, University Medical Center Hamburg-Eppendorf, 20246 Hamburg, Germany

**Keywords:** auditory, ferret, local field potential, midbrain, visual

## Abstract

The integration of visual and auditory spatial information is important for building an accurate perception of the external world, but the fundamental mechanisms governing such audiovisual interaction have only partially been resolved. The earliest interface between auditory and visual processing pathways is in the midbrain, where the superior (SC) and inferior colliculi (IC) are reciprocally connected in an audiovisual loop. Here, we investigate the mechanisms of audiovisual interaction in the midbrain by recording neural signals from the SC and IC simultaneously in anesthetized ferrets. Visual stimuli reliably produced band-limited phase locking of IC local field potentials (LFPs) in two distinct frequency bands: 6–10 and 15–30 Hz. These visual LFP responses colocalized with robust auditory responses that were characteristic of the IC. Imaginary coherence analysis confirmed that visual responses in the IC were not volume-conducted signals from the neighboring SC. Visual responses in the IC occurred later than retinally driven superficial SC layers and earlier than deep SC layers that receive indirect visual inputs, suggesting that retinal inputs do not drive visually evoked responses in the IC. In addition, SC and IC recording sites with overlapping visual spatial receptive fields displayed stronger functional connectivity than sites with separate receptive fields, indicating that visual spatial maps are aligned across both midbrain structures. Reciprocal coupling between the IC and SC therefore probably serves the dynamic integration of visual and auditory representations of space.

## Introduction

External events usually give rise to inputs across a number of sensory modalities, providing the brain with a stream of information that encompasses the collective physical representation of the event. However, the underlying mechanisms by which the brain integrates parallel sensory streams to form a unified representation of the external world remains poorly understood. Previous studies have provided evidence that multiple sensory systems converge and interact not just in higher cortical areas, but also in early sensory cortical and subcortical structures (Stein & Wallace, 1996; Wallace *et al.*, 1996; Musacchia & Schroeder, 2009; King & Walker, 2012). Indeed, compiling evidence is leading to a model of multisensory integration where virtually all ‘unisensory’ signals are to a certain extent influenced by other sensory modalities, even at the earliest stages of sensory processing (Schroeder & Foxe, 2005). One striking example of such multimodal sensory interaction is the presence of visual and eye-position signals at various stages along the auditory pathway (Bizley *et al.*, 2007; Porter *et al.*, 2007; Bizley & King, 2009). This effect was most prominently studied in the inferior colliculus (IC) (barn owl: Bergan & Knudsen, 2009; monkey: Bulkin & Groh, 2012; Gruters & Groh, 2012). In contrast to the neighboring superior colliculus (SC), which is inherently a multisensory structure

(Stein & Meredith, 1993), the IC is an early auditory structure that appears to be modulated by other sensory modalities. Therefore, due to its centralized position in the auditory pathway, the IC is an ideal structure to investigate the mechanisms by which a classically unisensory pathway is influenced by other sensory modalities.

Anatomical tracing studies have shown that the IC receives direct visual inputs from the retina (Cooper & Cowey, 1990), the SC (Adams, 1980; Doubell *et al.*, 2000) and the visual cortex (Cooper & Young, 1976). In addition, the IC provides a dense auditory projection to the deeper layers of the SC (Jiang *et al.*, 1997). Therefore, the visual projection from SC to IC and the auditory projection from IC to SC collectively represent the anatomical substrate for early audiovisual interactions in the brain. However, the physiological correlate of this reciprocal anatomical connectivity remains unclear. In the present study, our aim was to identify the physiological signatures of functional interaction between the IC and SC, with primary focus on identifying the source of visual inputs to the IC, and elucidating the mechanism by which these inputs modulate local network activity. To address these questions, we recorded both stimulus-evoked and spontaneous local field potentials (LFPs) from the IC and SC simultaneously in anesthetized ferrets. In the IC, we found that visual stimuli modulate the phase of LFPs in two distinct frequency bands (6–10 and 15–30 Hz) and that the timing of visual responses across the midbrain suggests the superficial SC as the source of visual input. Functional connectivity analysis additionally indicates that the SC to IC visual projection is visuotopic. As the

Correspondence: Prof A. K. Engel, as above.  
E-mail: ak.engel@uke.de

Received 10 October 2014, revised 9 December 2014, accepted 3 January 2015

first such demonstration of functional connectivity between the IC and SC, these findings provide a physiological context for previously identified anatomical pathways, and underline the importance of early multisensory interactions in the brain.

## Materials and methods

The data presented in this study were collected from 20 simultaneous penetrations of the SC and IC in six adult female ferrets (*Mustela putorius furo*; Supplier: Euroferret-Dybbølsgade, Copenhagen, Denmark). All experiments were approved by the independent Hamburg state authority for animal welfare (BUG-Hamburg) and were performed in accordance with the guidelines of the German Animal Protection Law.

### Surgery

Animals were initially anesthetized with an injection of ketamine (15 mg/kg) and medetomidine (0.08 mg/kg). A glass tube was then placed in the trachea to allow artificial ventilation of the animal and supply isoflurane anesthesia (0.5–1%, 50:50 N<sub>2</sub>O/O<sub>2</sub> mix). To prevent dehydration throughout experiments, a cannula was inserted into the femoral vein to deliver a continuous infusion of 0.9% NaCl, 0.5% NaHCO<sub>3</sub> and pancuronium bromide (60 µg/kg/h). Body temperature was maintained at 38 °C with a heating blanket controlled by the animal's rectal temperature. In addition, heart rate and end-tidal CO<sub>2</sub> concentration were constantly monitored throughout the duration of experiments to maintain the state of the animal. The temporalis muscle was reflected, and a rectangular-shaped craniotomy was performed over the left posterior cortex. After careful removal of the dura, the cortex was covered with saline solution. To ensure monocular stimulation, the left eye was occluded. Finally, to prevent desiccation of the cornea, a contact lens was placed on the right eye. Experiments typically lasted between 24 and 36 h, after which the animal was deeply anesthetized with 5% isoflurane and killed with an overdose of potassium chloride.

### Electrophysiology

Neural activity in the SC and IC was recorded simultaneously with 2 × 16 channel dual-shank (100 µm electrode spacing, 500 µm inter-shank distance) and 1 × 32 channel single-shank (50 or 100 µm electrode spacing) silicon probes, respectively (NeuroNexus Technologies, Ann Arbor, MI, USA). All silicon probe contacts had a surface area of 413 µm<sup>2</sup>, providing optimal impedance for measuring LFP. Probes were advanced simultaneously towards the midbrain along stereotaxic coordinates. Desirable recording configurations were obtained when robust responses were evoked by visual stimuli on the SC probe and auditory stimuli on the IC probe. Broadband signals from silicon probes were digitized at 22 321.4 Hz and sampled with an AlphaLab SnR recording system (Alpha Omega Engineering, Ubstadt-Weiher, Germany). All subsequent analysis of neural data was performed offline after the completion of experiments.

### Sensory stimulation

To ensure controlled conditions for sensory stimulation, all experiments were carried out in a dark sound-attenuated anechoic chamber (Acoustair, Moerkapelle, Netherlands). Auditory stimuli were generated in Psychophysics Toolbox (Brainard, 1997), digitalized at 96 kHz and delivered with an RME soundcard (RME HDSPe AIO Intelligent Audio Solutions) and played through a Beyerdynamic T1

speaker located 15 cm from the animal's right ear. The sound delivery system was calibrated using a Brüel and Kjær free-field 4939 microphone coupled to a B&K 2670 preamp and 2690 amplifier. Auditory stimuli consisted of clicks and pure tones of 0.5 and 100 ms, duration respectively. Thirty-eight different pure tone frequencies were selected ranging from 500 to 32 000 Hz. Clicks and pure tones were presented at 65 dB. Click and pure tone interstimulus intervals were randomly drawn between 1500 and 2000 ms and 300 and 400 ms, respectively. Pure tones were ramped on and off with 15-ms cosine-square functions. Visual stimuli were generated using the Psychophysics Toolbox and presented on an LCD monitor (Samsung SyncMaster 2233, frame rate 60 Hz) placed 28.5 cm in front of the animal. Visual stimuli consisted of very large (40°) flashes for probing visual responses, and smaller flashes (8°) for quantifying visual spatial receptive fields (11 × 9 grid for mapping). Each flash stimulus lasted one frame, equating to a stimulus duration of 16.7 ms. The interstimulus interval for large flashes and receptive field mapping flashes was drawn randomly between 1500 and 2000 ms and 130 and 150 ms, respectively. Flashes had a luminance of 242.80 cd/m<sup>2</sup> and were presented against a black background (0.19 cd/m<sup>2</sup>).

### Data analysis

All offline data analysis of neural signals was performed using custom scripts in Matlab (The Mathworks, Natick, MA, USA). We examined the low-frequency component (<200 Hz) of extracellular fields, the LFP, which reflect the net sum of local post-synaptic potentials (Buzsáki *et al.*, 2012). LFPs were obtained by low-pass filtering broadband signals with a phase-preserving fourth-order Butterworth filter at 200 Hz and then downsampling signals to 1395.1 Hz. LFP response latencies were defined as the post-stimulus time where signals deviated by more than two standard deviations from pre-stimulus baseline activity. To analyse sensory responses with respect to their spectral components in a time-resolved manner, LFPs were convolved with a series of complex Morlet wavelets. To replicate the natural 1/*f* distribution of extracellular fields and ensure optimal spectral resolution, 30 logarithmically spaced wavelet frequencies were chosen between 4 and 200 Hz. On a trial-by-trial basis, LFP signals were convolved with wavelets from 1.5 s pre-stimulus to 1.5 s post-stimulus in 5-ms steps. To compute stimulus-related changes in spectral power, spectra were corrected for pre-stimulus baseline activity. The standard deviation of stimulus-related spectra were estimated by jackknife random sampling, and significant power changes were defined as time–frequency data points where the mean total power exceeded the pre-stimulus mean plus two times the estimated standard deviation. To quantify stimulus-locked LFP phase modulations, inter-trial phase coherence (ITC) was computed across all trials (Lachaux *et al.*, 1999). Briefly, for each time and frequency, the instantaneous LFP phase in each trial was projected onto a unit circle. The resultant length of the mean unit vector is a quantitative measure of phase consistency over trials, with values close to 0 and 1 indicating very low and very high phase correlation, respectively. The statistical significance of ITC values was determined by the Rayleigh statistic at a significance level of *P* < 0.01 (Fisher, 1993).

As we recorded neural activity from directly adjacent midbrain structures, we had to ensure that LFP responses observed in one structure were not the result of volume-conducted signals propagating from the neighboring structure. Spectral coherence is a measure of the consistency of phase coupling between simultaneously recorded signals and comprises both real and imaginary parts. The imaginary part of coherence was chosen instead of conventional

coherence because it quantifies exclusively non-zero phase-lagged components, thereby eliminating volume-conducted signals which propagate with zero phase lag (Nolte *et al.*, 2004). The value of the imaginary part of coherence is bound between  $-1$  and  $1$ , and is determined by the relative phase shift between signals. However, for greater simplicity, the absolute value of imaginary coherence was used for plotting and population analysis. The statistical significance of imaginary coherence values was determined by methods outlined by Nolte *et al.* (2004). The phase-slope index (PSI) was used as a quantitative measure of the relative latencies of phase-locked signals between the SC and IC (Nolte *et al.*, 2008). Unlike coherence, which is measured for each time point and frequency, PSI measures the relative phase-lag of signals across frequency bands, with the sign of the 'phase slope' indicating the directionality of interaction. PSI values were subsequently transformed into units of standard deviation, as estimated by jackknife random sampling.

## Results

### Physiological reconstruction of recording position in the SC and IC

As both the SC and the IC can be further divided into anatomically and functionally distinct subregions, we analysed sensory responses with respect to the intrinsic organization of each structure. For this we first identified physiological markers of the placement of electrodes relative to the main landmarks of the SC and IC. In a previous study, we identified a flash-evoked physiological marker in the SC (Stitt *et al.*, 2013), termed the current source density inflection depth (ID), which corresponds approximately to the anatomical

border between the stratum griseum superficiale (SGS) and the stratum opticum (SO) (Fig. 1B). ID was consistent across recording sessions and animals and was therefore used to align all SC penetrations post-hoc to enable layer-specific analysis of neural responses. As the stratum opticum spans approximately  $200\ \mu\text{m}$  dorsoventrally in the ferret, we presumed the location of the anatomical subdivision between superficial and deep SC layers to be  $200\ \mu\text{m}$  below the current source density ID (Stitt *et al.*, 2013).

In contrast to the SC, which is composed of several layers, the most relevant landmark in the IC is the border between the external nucleus and the tonotopically organized central nucleus. Reflecting the tonotopy of the central nucleus, we consistently observed high-frequency ( $40\text{--}80\ \text{Hz}$ ) fluctuations in LFP power that were tuned to the frequency of pure tone stimuli, with the strong tendency for the best frequency to increase with recording depth (Fig. 1C). As the external capsule of the IC displays little or no frequency preference (Aitkin *et al.*, 1975), we selected the most superficial frequency-tuned recording contact as a physiological marker to approximate the anatomical border between the external capsule and central nucleus of the IC. All subsequent depth-wise analysis of neural activity in the IC is presented with respect to this marker. Penetrations where no frequency tuning was detected on any recording contact were omitted from analysis.

### Flash- and click-evoked responses in the SC

We detected flash-evoked responses in LFPs across the entire dorsoventral extent of the SC, with the largest amplitude responses occurring around the inflection depth, in the superficial SC (Fig. 2A). In contrast, click-evoked event-related potentials (ERPs) were lower in

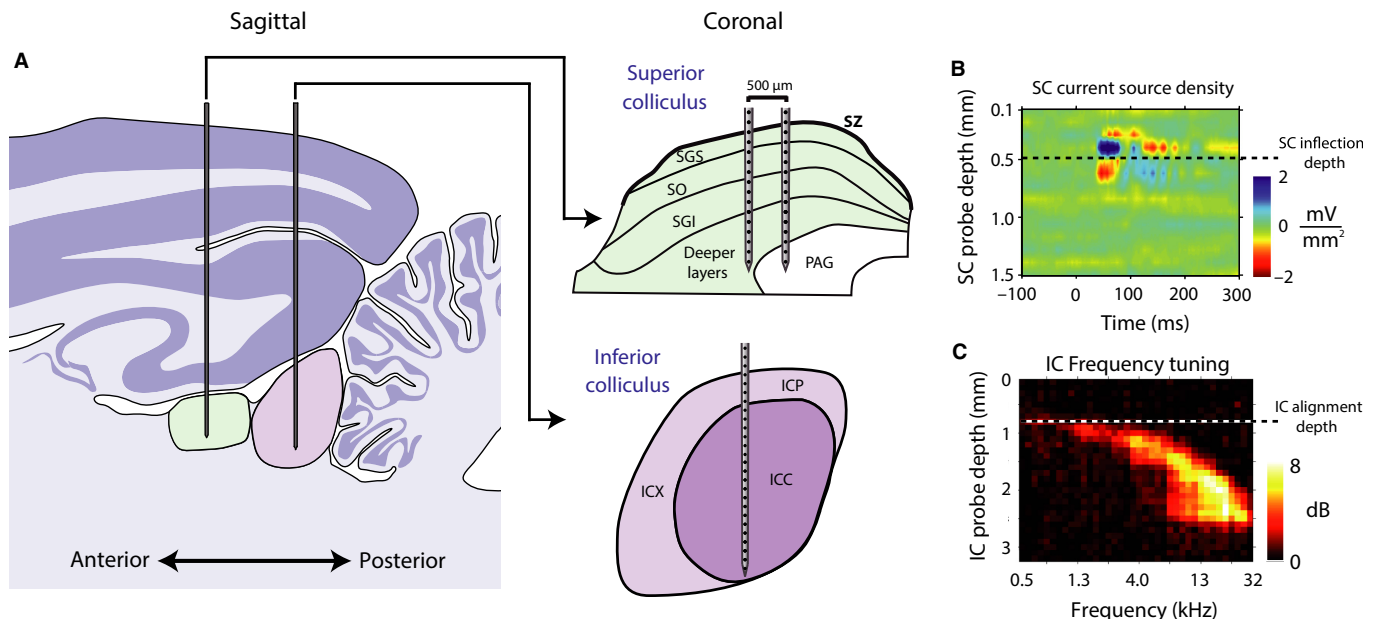


FIG. 1. Electrode placement and penetration reconstruction. (A) A dual-shank ( $16 \times 2$ ) multichannel linear probe was placed in the SC such that electrodes spanned as many layers as possible. In addition, a single-shank ( $1 \times 32$ ) multichannel linear probe was placed in the IC such that electrodes spanned both the central nucleus and the external capsule. (B) In the SC, the inflection depth of flash ERPs, or border between current source and sink, reflects the anatomical border between the two superficial SC layers, the SGS and SO. The inflection depth was used to align all penetrations for depth-wise population analysis. Flash ERPs were computed from 400 stimulus repetitions. (C) Frequency tuning profile of an example IC penetration. The color bar in the frequency tuning matrix represents the strength of evoked gamma power following pure tone stimuli. Pure tone responses were computed from 100 stimulus repetitions of each pure tone frequency. Note that best frequency increases gradually with recording depth in the IC. The most superficial frequency-tuned recording site was presumed to reflect the approximate anatomical border between the external capsule and central nucleus in the IC, and was used to align all penetrations for depth-wise analysis. SZ, stratum zonale; SGS, stratum griseum superficiale; SO, stratum opticum; SGI, stratum griseum intermediale; PAG, periaqueductal gray; ICP, pericentral nucleus of the inferior colliculus; ICX, external nucleus of the inferior colliculus; ICC, central nucleus of the inferior colliculus.

amplitude and focused in the deep layers of the SC. To investigate flash and click responses in more detail, we analysed stimulus-related changes in LFP power and phase locking, which quantify the amplitude and temporal dependence of LFP responses, respectively. Spectral responses to flashes in the SC were typically characterized by large increases in signal power and phase locking in frequencies above 10 Hz (Fig. 2C and E), and were strongest in superficial layers (Fig. 4A). The mean ( $\pm$  SD) latency of visual responses was  $31.9 \pm 10$  ms in superficial SC layers and  $39.2 \pm 17.2$  ms in deep SC layers. Spectral responses to clicks were characterized by power increases in high spectral frequencies and significant phase locking across a broader range of LFP frequencies in deep SC layers (Figs 2D and F, and 4B). Click response latencies

were  $30.1 \pm 25.2$  ms in superficial layers and  $16.2 \pm 18$  ms in deep layers. A depth-resolved analysis of flash and click responses across all SC penetrations is presented in Fig. 4.

*Flash- and click-evoked responses in the IC*

IC penetrations were characterized by robust responses to clicks and pure tones usually detected on distributed probe contacts spanning up to 2.5 mm dorsoventrally (Fig. 3A). Click ERPs displayed brief upward and downward deflecting components, with the positive deflecting component more pronounced in superficial regions, and the negative deflecting component in deeper regions (Fig. 4D). Click responses occurred much faster than flash responses in the IC (click

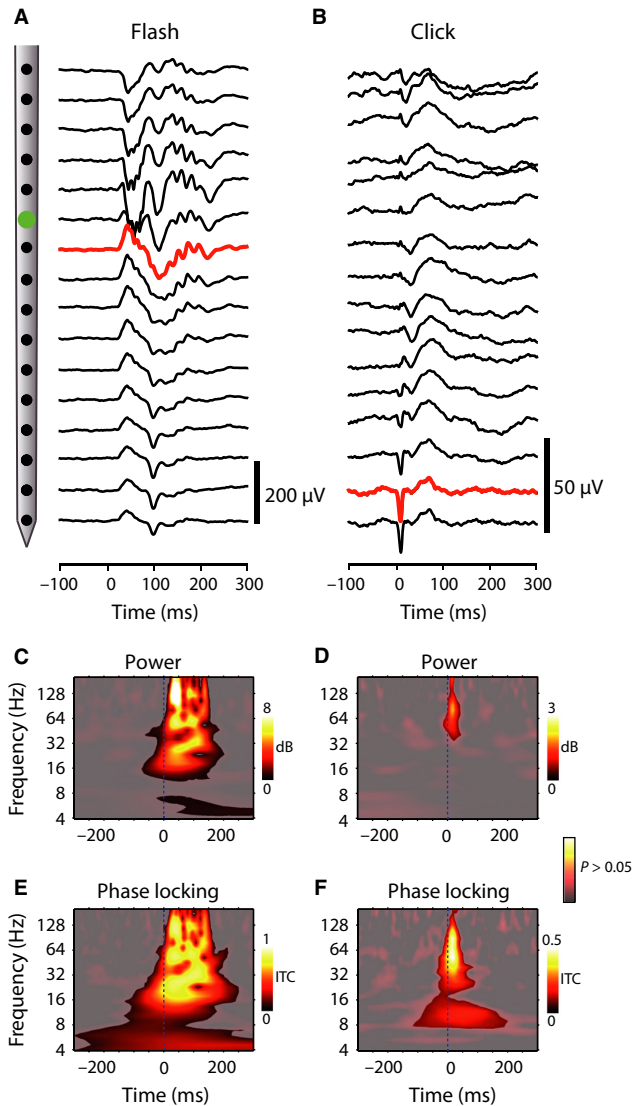


FIG. 2. Flash- and click-evoked responses in the SC. (A, B) Flash and click ERPs for all 16 probe contacts from one example SC penetration. The recording contact corresponding to the inflection depth is marked in green. The responses shown in C–F are taken from the recording contacts plotted in red. (C, D) Total power spectrograms following flashes and clicks. (E, F) Inter-trial phase coherence spectrograms quantifying LFP phase locking to flash and click stimuli. LFP responses were computed from 400 repetitions of flash and click stimuli. The level of significance for power and inter-trial phase coherence spectrograms is displayed by a transparency mask ( $P < 0.05$ ). ITC, inter-trial coherence.

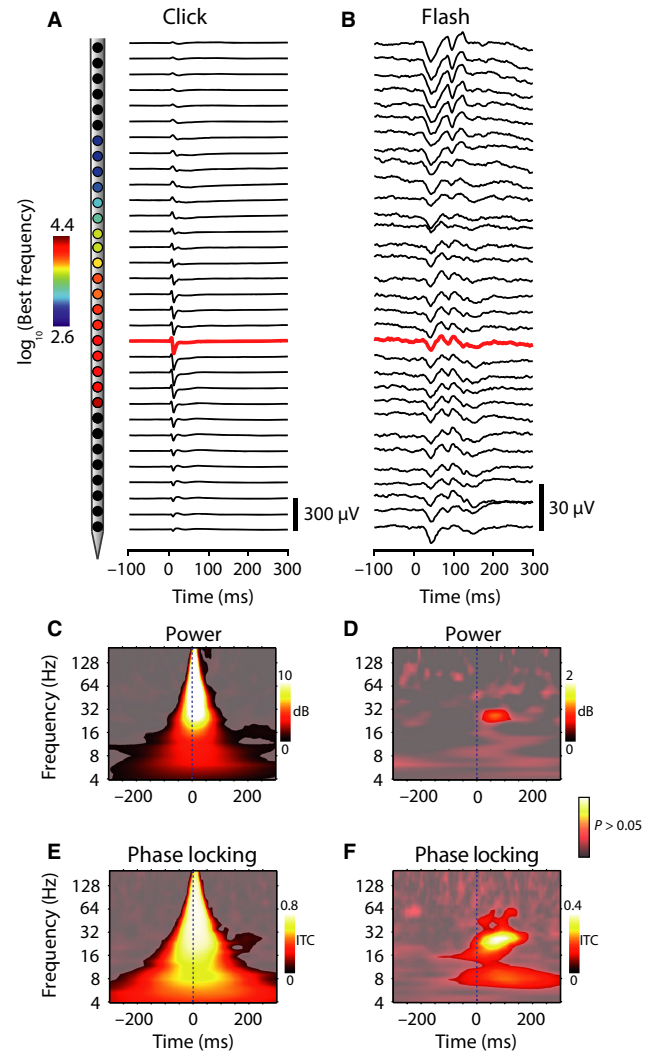


FIG. 3. Click- and flash-evoked responses in the IC. (A, B) Click and flash ERPs for all 32 probe contacts on from one example IC penetration. The best frequency for tonotopic recording sites is displayed in A. Spectral analyses shown in C–F are presented for the responses plotted in red. (C, D) Total power spectrograms following clicks and flashes. (E, F) Inter-trial phase coherence spectrograms quantifying LFP phase locking to click and flash stimuli. Note the presence of significant phase locking to flash stimuli in the 6–10 and 15–30 Hz frequency bands. LFP responses were computed from 400 repetitions of flash and click stimuli. The level of significance for power and inter-trial phase coherence spectrograms is displayed by a transparency mask ( $P < 0.05$ ). ITC, inter-trial coherence.

latency  $7.5 \pm 4.9$  ms, flash latency  $34.2 \pm 6.3$  ms). Spectral responses to clicks in the IC were characterized by very large and significant increases in power and phase locking across all measured LFP frequencies (Fig. 3C and E). In contrast, flash responses in the IC were characterized by low-amplitude periodic deflections in ERPs (Fig. 3B) that were consistently observed across all penetrations (Fig. 4C). Figure 3 displays the spectral analysis of flash-evoked LFP responses from one example recording contact in the IC. In this example, flashes evoked small change in LFP signal power (Fig. 3D), but rather strong and highly significant ITC in two distinct frequency bands: 6–10 and 15–30 Hz (Fig. 3F).

*Flash stimuli preferentially modulate LFP phase and not power in the IC*

To investigate if IC visual responses across all recording sites displayed similar spectral characteristics to the example shown in

Fig. 3, we computed the average flash-evoked increase in power and phase locking across all IC recording contacts (Fig. 5). We found that 8% ( $0.13 \pm 0.02$  dB, population average  $\pm$  SEM) and 16% ( $0.31 \pm 0.02$  dB) of IC recording sites displayed significant power changes in the 6–10 and 15–30 Hz frequency bands, respectively ( $P < 0.05$ ). In contrast, 64% ( $0.14 \pm 0.004$  ITC) and 62% ( $0.18 \pm 0.005$  ITC) of IC recording sites displayed significant phase locking in the 6–10 and 15–30 Hz frequency bands, indicating that flash stimuli preferentially modulate the phase of LFPs and not power. In contrast to flashes, click stimuli consistently evoked significant changes in both power (76% of the sites;  $4.74 \pm 0.20$  dB) and phase locking (91% of the sites;  $0.91 \pm 0.01$  ITC) in the 40–80 Hz frequency range (Fig. 5C and D). To compare visual responses between the central and external nuclei of the IC, we grouped recording sites into frequency tuned and untuned groups. Untuned recording sites displayed significantly stronger phase locking in both the 6–10 Hz ( $0.12 \pm 0.006$  ITC tuned, vs.

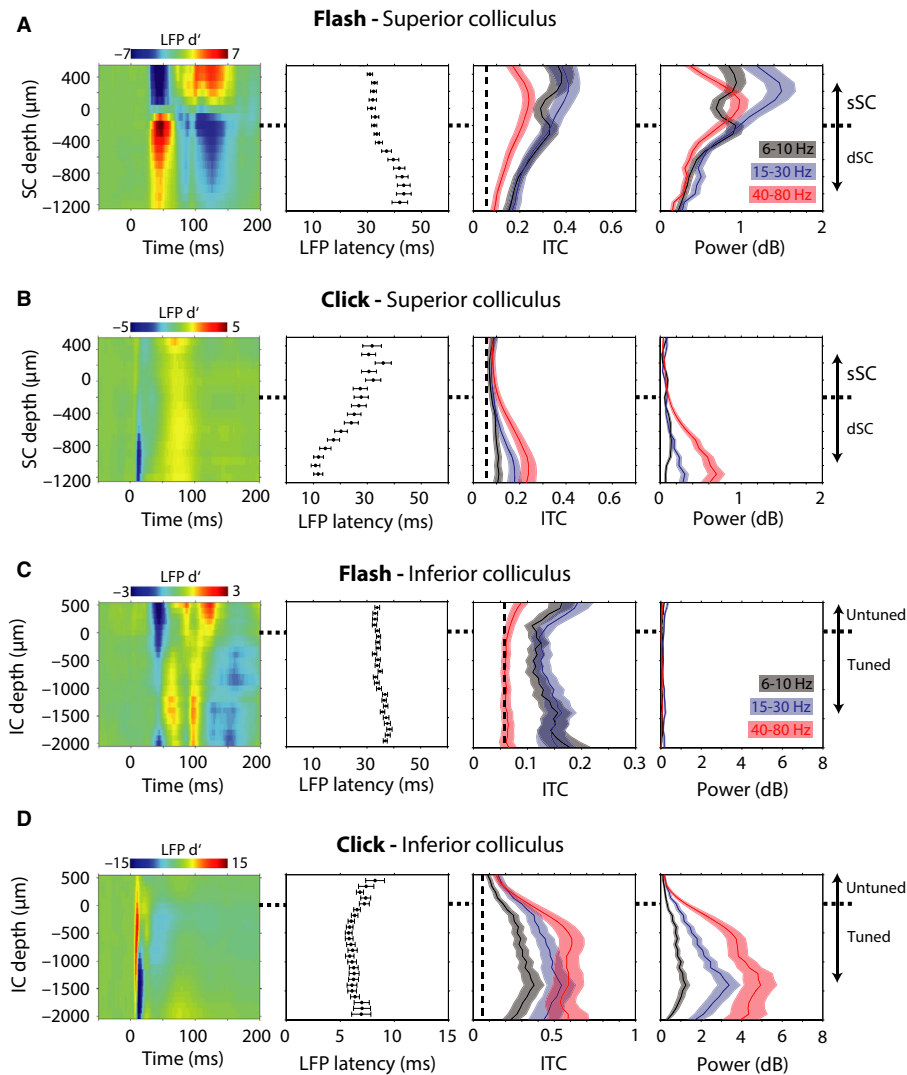


FIG. 4. Depth-resolved measures of sensory responses across all SC and IC penetrations. From top to bottom, each row displays depth-resolved population average responses to flashes (A) and clicks (B) in the SC, and flashes (C) and clicks (D) in the IC. The left column displays the population-averaged ERPs, expressed in terms of standard deviation from the prestimulus baseline. The second column displays the latency of LFP responses  $\pm$  standard error of the mean. The third column shows inter-trial phase coherence, where the level of significant phase locking is shown as a dotted line ( $P < 0.05$ ). The right column displays stimulus-evoked power. Depth of 0  $\mu\text{m}$  in SC plots indicates the presumed SGS/SO border, with the superficial/deep subdivision located 200  $\mu\text{m}$  lower. Depth of 0  $\mu\text{m}$  in IC plots indicates the presumed external/central nucleus border. Spectral analysis was performed in three distinct frequency bands: 6–10, 15–30 and 40–80 Hz. Population responses were computed from 40 penetrations of the SC, and 20 penetrations of the IC.

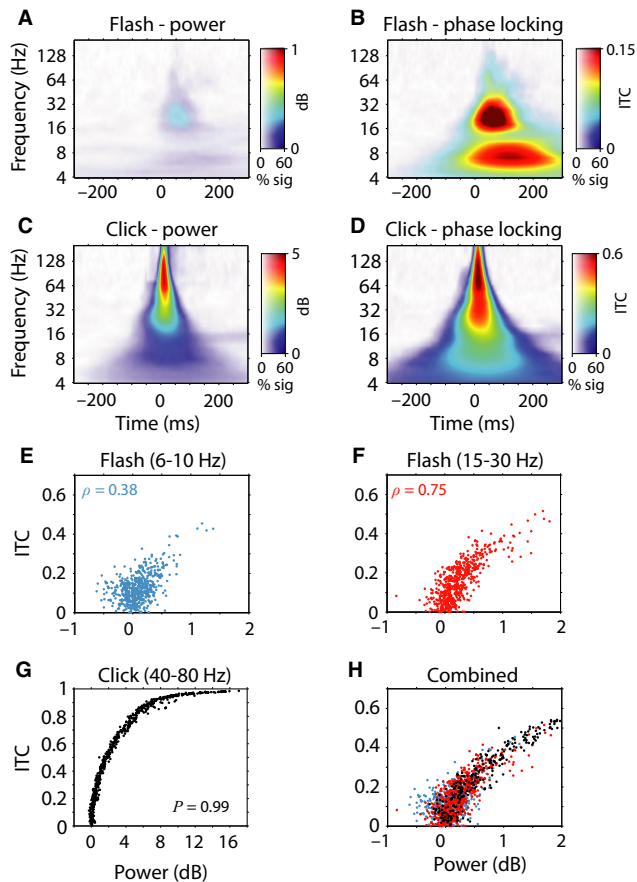


FIG. 5. Flash and click population spectrograms in the IC. (A) The population-averaged power spectrogram for flash stimuli. Note the absence of any large or significant increases in power associated with flashes. (B) The population-averaged inter-trial phase coherence spectrogram for flash stimuli. Note the large amplitude and highly significant phase locking in two distinct frequency bands: 6–10 and 15–30 Hz. (C) Population-averaged total power spectrogram for click stimuli. (D) Population-averaged inter-trial phase coherence spectrogram for click stimuli. Note the large and highly significant power and phase locking in almost all LFP frequencies following click stimuli. In each spectrogram plot, average spectra are covered with a transparency mask denoting the percentage of recording sites with significant power or phase modulations ( $P < 0.05$ ). (E, F) Flash-evoked power plotted against the strength of phase locking for all IC recording sites in the 6–10 and 15–30 Hz frequency bands. Note the strong positive correlation between power and phase locking for both phase-locked frequency bands. (G) Click-evoked power plotted against the strength of phase locking. (H) Data from E–G displayed together on the same plot. In each plot,  $\rho$  denotes the Spearman correlation coefficient, which was significant in all plots ( $P < 0.001$ ).

$0.15 \pm 0.005$  ITC untuned) and 15–30 Hz ( $0.14 \pm 0.006$  tuned, vs.  $0.18 \pm 0.006$  untuned) frequency bands ( $P = 1.03 \times 10^{-6}$ , 1 degree of freedom,  $F$  statistic = 24.51).

Previous studies have interpreted phase locking in the absence of changes in signal power as evidence for a stimulus-induced phase reset of ongoing brain oscillations, implying that phase reset and evoked power responses originate from two fundamentally different biophysical processes (Makeig *et al.*, 2002; Lakatos *et al.*, 2007; Sieben *et al.*, 2013). To investigate the relationship between stimulus-related changes in LFP signal power and phase locking in more detail, we plotted the strength of evoked power against phase locking for all IC recording sites for flash and click stimuli (Fig. 5E–G). Although phase locking best characterized visual responses in the IC, visual evoked power and phase locking were positively correlated in both the 6–10 Hz (Spearman correlation = 0.38,  $P = 0$ ) and

15–30 Hz (Spearman correlation = 0.75,  $P = 2.68 \times 10^{-89}$ ) frequency bands. Therefore, recording contacts that displayed strong phase locking to flash stimuli also displayed proportionally larger increases in LFP power. Similarly, click responses displayed a very tight correlation between evoked power and phase locking in the 40–80 Hz frequency band (Spearman correlation = 0.99,  $P = 0$ ). Despite click stimuli displaying a much larger range of power values, when plotted together, the underlying relationship between evoked power and phase locking was indistinguishable for flash and click responses in the IC (Fig. 5H).

#### Visually evoked LFP phase locking is intrinsic to the IC

For the most part, LFPs reflect the net sum of post-synaptic potentials of neurons in tissue immediately surrounding the recording electrode (Buzsáki *et al.*, 2012). However, large and highly synchronous events can be recorded at greater distances from recording electrodes due to the effects of volume conduction. Therefore, to confirm the local origin of visually evoked activity in the IC, we had to ensure that responses were not spuriously produced by volume-conducted signals originating from the directly adjacent and highly visually sensitive SC. As we recorded neural activity from the SC and IC simultaneously, we were able to specifically test if IC visual responses were volume-conducted signals by computing the imaginary part of coherence between co-recorded SC and IC LFPs (see Methods). As superficial and deep SC layers receive bottom-up retinal and top-down cortical visual inputs respectively, we analysed imaginary coherence for superficial SC to IC and deep SC to IC channels separately. The flash-evoked imaginary coherence spectrogram computed between all pairs of superficial SC and IC recording contacts revealed non-zero phase coherence in the 15–30 Hz frequency band ( $0.12 \pm 0.002$ , 65% significant channel pairs, Fig. 6A). Deep SC and IC channel pairs displayed a similar effect with slightly lower magnitude ( $0.09 \pm 0.001$ , 53% significant channel pairs, Fig. 6B). As SC and IC visual responses display LFP phase consistency at a non-zero phase angle, these data indicate that IC flash-evoked LFP responses in the 15–30 Hz frequency band are not the product of volume-conducted signals from the SC. In contrast, the lower 6–10 Hz phase-locked frequency band showed weak imaginary coherence computed for both superficial SC to IC ( $0.05 \pm 0.001$ , 26% significant channel pairs) and deep SC to IC ( $0.07 \pm 0.001$ , 39% significant channel pairs) recording contact pairs. The comparatively weak imaginary coherence in the 6–10 Hz frequency band indicates that SC and IC visual responses in this band display almost zero phase-lag. As one cannot distinguish between true physiological interaction and spurious interaction produced by volume conduction from zero phase-lagged signals, visual responses in the 6–10 Hz frequency band were not considered for further analysis. For comparison, click-evoked responses displayed strong imaginary coherence between the IC and deep SC for LFP frequencies above 20 Hz ( $0.16 \pm 0.002$ , 61% significant channel pairs, Fig. 6E) and comparatively weak coherence with superficial SC ( $0.07 \pm 0.001$ , 36% significant channel pairs, Fig. 6D).

#### The temporal order of flash and click responses in the midbrain

To gain a better understanding of the relative timing of sensory responses in the midbrain, we computed the stimulus-evoked PSI between SC and IC LFPs. In this context, the PSI returns a score that indicates the strength with which phase-locked signals from

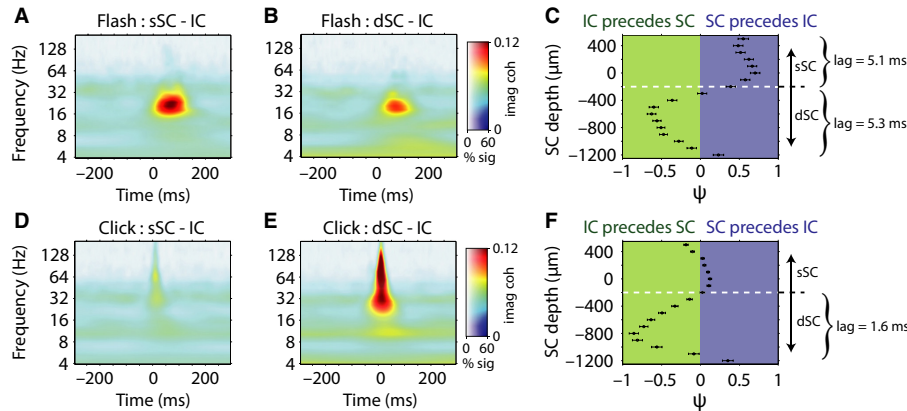


FIG. 6. Imaginary coherence and temporal order of sensory responses in the midbrain. (A) Population-averaged flash-evoked imaginary coherence spectrogram computed between superficial SC and IC recording contacts. (B) Population-averaged flash-evoked imaginary coherence spectrogram computed between deep SC and IC recording contacts. Note the presence of significant non-zero coherence in the 15–30 Hz frequency band following flash stimuli for both superficial and deep SC recording sites. (C) The average ( $\pm$  SEM) flash-evoked PSI computed between SC channels at varying depths and IC channels. Positive PSI values indicate that the SC precedes the IC, and negative values that the IC precedes the SC. Note the flip in temporal order of visual responses around the superficial/deep border in the SC. (D) Population-averaged click-evoked imaginary coherence spectrogram computed between superficial SC and IC. (E) Population-averaged click-evoked imaginary coherence spectrogram computed between deep SC and IC. Note the strength of click-evoked coherence in higher LFP frequencies between deep SC and IC recording sites. (F) Mean ( $\pm$  SEM) click-evoked PSI between SC and IC channels. Note that auditory responses in deep layers of the SC are consistently preceded by responses in the IC.

each structure precede or follow each other, with positive values indicating that SC leads IC, and negative values that IC leads SC. Visually evoked PSI values were computed across the phase-locked 15–30 Hz frequency band. Visual responses in the superficial SC consistently preceded IC responses with an average phase lag of  $5.1 \pm 0.2$  ms (Fig. 6C). However, transitioning from superficial to deep SC, the polarity of PSI values flips such that IC visual responses precede deep SC responses by  $5.3 \pm 0.4$  ms. Taken together, these data indicate that flash responses in the 15–30 Hz frequency band occur first in superficial SC, then in IC and finally in the deep SC. Click-evoked responses were generally composed of much higher LFP frequency components than flash responses (Fig. 5), and therefore we computed click-evoked PSI values in the 80–150 Hz frequency band. IC responses consistently preceded deep SC responses with an average phase lag of  $1.6 \pm 0.03$  ms (Fig. 6F), with no effect in superficial SC layers. It should be emphasized that these PSI results do not quantify stimulus-evoked SC–IC functional connectivity but, rather, the temporal order of stimulus-evoked responses across these midbrain structures.

#### Overlap of SC and IC visual receptive fields predicts the strength of spontaneous functional connectivity

In ten penetrations from three animals, we quantified visual spatial receptive fields in the SC and IC using the strength of flash-evoked phase locking in the 15–30 Hz frequency band (Fig. 7). IC receptive fields were often very large, encompassing the majority of the contralateral visual field (width  $41 \pm 2.1^\circ$  and height  $28 \pm 1.3^\circ$  (mean  $\pm$  SEM)). We reasoned that if the SC provided visual input to the IC, then co-recorded SC and IC regions with overlapping visual spatial receptive fields should display greater functional connectivity at rest compared with regions with non-overlapping receptive fields. In the preceding sections, we have presented the analysis of stimulus-related LFPs. However, it is difficult to infer functional connectivity solely from responses to transient stimuli such as flashes and clicks, as one cannot distinguish phase correlations resulting from true interaction and those spuriously produced through shared temporal entrainment via sensory stimulation. To

overcome this, we computed imaginary coherence between SC and IC channel pairs in the 15–30 Hz frequency band for spontaneously recorded LFPs. Figure 7C displays spontaneous imaginary coherence plotted against the similarity of visual spatial receptive fields. Receptive field similarity was quantified as the correlation coefficient between SC and IC spatial receptive field maps. There was a highly significant positive correlation between receptive field similarity and spontaneous SC–IC imaginary coherence ( $R = 0.26$ ,  $P < 0.0001$ ), confirming that retinotopically similar recording sites in the SC and IC are more functionally coupled, even in the absence of sensory stimulation.

#### Discussion

This study represents the first attempt to identify the physiological signatures of early audiovisual interaction in the midbrain through simultaneous recording of SC and IC neural activity. We systematically assessed visual and auditory LFP responses as a function of the laminar organization of each midbrain structure. The results of this study demonstrate that visual stimuli modulate IC LFPs in the anesthetized ferret. IC visual responses were characterized by phase locking of LFP oscillations in the 6–10 and 15–30 Hz frequency bands. Although responses were found throughout the IC, they were strongest for untuned recording sites located in the presumed external nucleus. IC visual responses occurred slightly later than responses in the superficial SC, but slightly earlier than responses in the deeper SC layers, suggesting that visual responses were neither the product of direct retinal or cortical inputs. Indeed, functional connectivity analysis performed on spontaneous LFPs strongly points to the SC as the source of visual inputs to the IC. This suggests that the SC to IC projection may represent the point of entry for visual information into both the ascending and the descending auditory pathways.

#### Non-auditory activity in the IC

Previous studies have identified visually evoked activity from the IC in anesthetized cats (Tawil *et al.*, 1983; Mascetti & Strozzi, 1988),

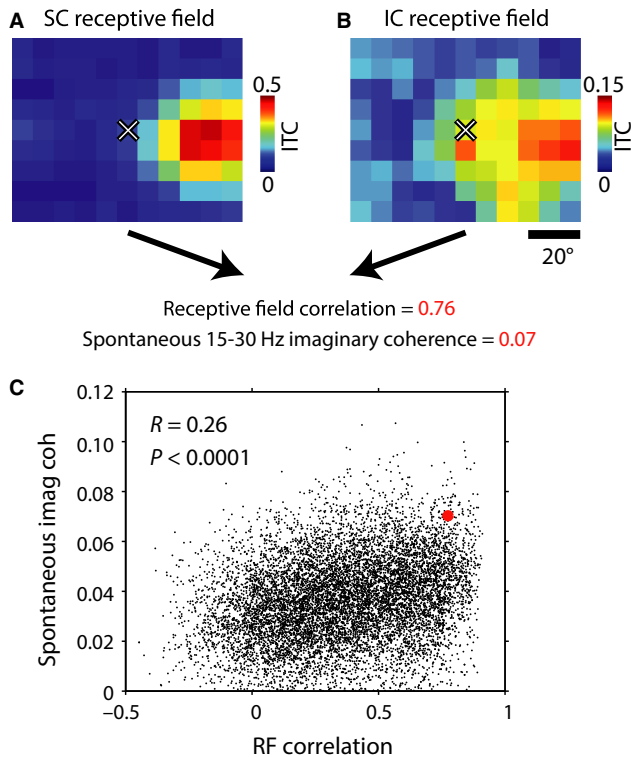


FIG. 7. Correlation of receptive field similarity and spontaneous coherence. (A,B) Visual receptive fields in the SC (A) and IC (B) from one example recording. Receptive fields were quantified using the strength of inter-trial phase coherence in the 15–30 Hz frequency band. (C) A scatter plot of all SC–IC channel pair combinations ( $n = 10\,240$ ) with receptive field similarity on the  $x$ -axis and the strength of spontaneous imaginary coherence in the 15–30 Hz band on the  $y$ -axis. The data point representing the channel pair shown above is plotted in red. Note the highly significant positive correlation between receptive field similarity and spontaneous coherence.

owls (Gutfreund *et al.*, 2002; Bergan & Knudsen, 2009) and awake behaving monkeys (Porter *et al.*, 2007; Bulkin & Groh, 2012). In addition, Groh and colleagues found that IC neurons in monkeys also carry saccade- (Porter *et al.*, 2007) and eye position-related signals (Groh *et al.*, 2001; Porter *et al.*, 2006). Similar to our results, Bulkin & Groh (2012) found that the prevalence of non-auditory activity in the IC was higher in the external nucleus than in the tonotopically organized central nucleus. However, the functional relevance of visual activity at the level of the IC remains poorly understood. One prominent idea is that audiovisual interaction at the level of the mid-brain acts as an interface for the co-registration of visual and auditory space (Gruters & Groh, 2012). Our finding that retinotopically similar recording sites in the SC and IC display stronger functional connectivity is consistent with the hypothesis that this projection carries visual spatial signals. Indeed, Hyde & Knudsen (2002) showed that auditory spatial maps in the owl IC were displaced in animals that were raised wearing optical prisms over their eyes, suggesting that visual inputs ensure the alignment of sensory maps by informing auditory spatial plasticity in the IC. However, unlike owls, ferrets and primates move their eyes relative to their heads, indicating that a different and highly adaptive mechanism is required for the alignment of visual and auditory space. Groh *et al.* (2001) provided evidence for this mechanism by showing that eye-position signals modulate the amplitude of auditory responses in monkey IC neurons, with maximum amplitude responses occurring when the animal's gaze was in the contralateral visual hemifield. The gain modulation

of auditory responses by eye position was independently confirmed by Zwiers *et al.* (2004), although this study reported no systematic spatial preference for modulatory effects. While in agreement on the gain modulatory effects of visual stimulation on auditory responses in the IC, the two studies mentioned above present contrasting results regarding the eye-position-mediated gain modulation of spontaneous activity of IC neurons, where Groh *et al.* (2001) found that eye position modulated spontaneous firing rate and Zwiers *et al.* (2004) found no effect on spontaneous activity. The discrepancy regarding the modulation of spontaneous IC activity by eye position has important implications for understanding the underlying mechanisms of cross-modal gain modulation. On the one hand, multisensory effects could be explained by a generalized modulation of excitability controlled by eye position yielding gain modulation of spontaneous and stimulus-related activity. On the other hand, modulatory effects might be produced by the non-linear combination of auditory, visual and eye-position information, thus precluding gain modulation of ongoing activity. Nevertheless, the fact that visual and/or eye position inputs converge at such an early stage of auditory processing highlights how important the integration of the various sensory modalities is in the brain.

#### Functional connectivity in the midbrain

Anatomical tracing studies have identified a number of potential sources of visual input to the IC, including the contralateral retina (rat: Itaya & Van Hoesen, 1982; Yamauchi & Yamadori, 1982; cat: Cooper & Cowey, 1990; mole-lemming: Herbin *et al.*, 1994), the superficial and deep layers of the SC (cat: Adams, 1980; rat: Coleman & Clerici, 1987; bat: Covey *et al.*, 1987; ferret: Doubell *et al.*, 2000), and the visual cortex (cat: Cooper & Young, 1976). Collectively, these bottom-up and top-down inputs presumably work in unison in behaving animals to modulate auditory spatial signals in the IC. Indeed, the multiple peaks and troughs visible in flash-evoked potentials in the IC suggest that several temporally shifted sources of input drive IC visual activity. However, physiological evidence reported here suggests the SC as the primary driver of visually evoked activity in the IC. Such temporally shifted peaks and troughs in IC ERPs may reflect the subsequent activation of the various input pathways to the SC, such as fast-conducting Y-type and slow-conducting W-type retinal ganglion cells, as well as corticotectal inputs (Freeman & Singer, 1983; Berson, 1988; Waleszczyk *et al.*, 2004; Manger *et al.*, 2010). Doubell *et al.* (2000) provided further evidence that the SC drives visual activity in the IC by showing that electrical stimulation of the superficial SC *in vitro* evokes excitatory postsynaptic potentials (EPSPs) in IC neurons. The latencies of electrically evoked monosynaptic EPSPs *in vitro* are slightly longer than the relative phase lag of SC and IC visual responses reported here (5 ms *in vivo*; 7 ms *in vitro*). However, when axon conductance is corrected for the lower recording temperature of *in vitro* preparations then electrically and stimulus-evoked latencies are in strong agreement (Franz & Iggo, 1968). In the opposite direction, auditory inputs from the IC converge on deep SC layers to form a map of auditory space that is aligned with the retinotopic visual map in superficial SC layers (Stein & Meredith, 1993; King *et al.*, 1998). The alignment of visual and auditory maps between deep and superficial SC layers is highly dynamic, with the representation of auditory space constantly readjusted to account for eye movements (Populin & Yin, 2002). Such flexible realignment of sensory spatial maps across SC layers could be achieved by using visual and eye position inputs from the SC to inform the gain modulation of bottom-up IC auditory signals.

### Sensory-evoked LFP phase modulation as a mechanism for multisensory interaction

Previous studies have interpreted the coexistence of insignificant changes in signal power and significant phase locking as evidence for the stimulus-evoked reorganization of the phase of ongoing LFP oscillations (Makeig *et al.*, 2002). Our data demonstrate that visually evoked LFP responses in the IC match these criteria. This is in line with previous findings from auditory cortex in monkeys, where somatosensory (Lakatos *et al.*, 2007) and visual stimuli (Kayser *et al.*, 2008; Lakatos *et al.*, 2009) have been shown to modulate the phase of ongoing LFPs. Similar phase modulation has also been observed in the somatosensory cortex in mice (Sieben *et al.*, 2013) and the visual cortex in humans (Naue *et al.*, 2011). Although the mechanism of oscillatory phase reset has often been postulated, few studies have thoroughly investigated this phenomenon from a neurophysiological perspective. As we have shown here, it is very difficult to disentangle phase modulations from changes in power as these two variables are so tightly interdependent for responses to transient stimuli. We believe that, rather than signifying a reset in oscillatory phase, the presence of stimulus-evoked phase locking in the apparent absence of power change simply reflects the greater sensitivity of phase locking measures for quantifying weak LFP responses. Conceptually, any barrage of sensory-evoked inputs will produce synchronous postsynaptic potentials in target neurons that would be detectable as amplitude fluctuations in electrical fields (Buzsáki *et al.*, 2012). That is to say, even if inputs act to reset the phase of ongoing oscillations, changes in the power of LFPs are unavoidable. Perhaps a more adept measure should be developed that encompasses both stimulus-evoked power and phase locking, to avoid further confusion surrounding the underlying biophysical processes that govern stimulus-evoked responses in the brain.

In conclusion, this study demonstrates that the IC displays weak visual responses in the anesthetized ferret, with visual inputs probably originating from a retinotopic SC-to-IC projection. Taken together with previous work on the IC-to-SC auditory projection, our data provide evidence for the physiological substrate for early audiovisual interactions in the brain. Rather than integrating complex features of visual and auditory inputs, such interaction probably serves the dynamic integration of eye-centric and head-centric representations of visual and auditory space. However, further studies in awake and behaving animals are required to elucidate the precise function of audiovisual interaction in the midbrain.

### Acknowledgements

We thank Jennifer Groh and Kurtis Gruters for comments on the manuscript, Dorrit Bystron for her assistance throughout experiments, and Guido Nolte for guidance with data analysis. This research was supported by funding from the DFG (GRK 1247/1–2; SFB 936/A2; SPP 1665/EN/533/13–1; A.K.E.).

### Abbreviations

EPSP, excitatory postsynaptic potential; ERP, event-related potential; IC, inferior colliculi; ID, inflection depth; ITC, inter-trial phase coherence; LFP, local field potential; PSI, phase-slope index; SC, superior colliculi; SGS, stratum griseum superficiale; SO, stratum opticum.

### References

Adams, J. (1980) Crossed and descending projections to the inferior colliculus. *Neurosci. Lett.*, **19**, 1–5.

- Aitkin, L., Webster, W., Veale, J. & Crosby, D. (1975) Inferior colliculus. I. Comparison of response properties of neurons in central, pericentral, and external nuclei of adult cat. *J. Neurophysiol.*, **38**, 1196–1207.
- Bergan, J.F. & Knudsen, E.I. (2009) Visual modulation of auditory responses in the owl inferior colliculus. *J. Neurophysiol.*, **101**, 2924–2933.
- Berson, D.M. (1988) Retinal and cortical inputs to cat superior colliculus: composition, convergence and laminar specificity. *Prog. Brain Res.*, **75**, 17–26.
- Bizley, J.K. & King, A.J. (2009) Visual influences on ferret auditory cortex. *Hearing Res.*, **258**, 55–63.
- Bizley, J.K., Nodal, F.R., Bajo, V.M., Nelken, I. & King, A.J. (2007) Physiological and anatomical evidence for multisensory interactions in auditory cortex. *Cereb. Cortex*, **17**, 2172–2189.
- Brainard, D. (1997) The psychophysics toolbox. *Spatial Vision*, **10**, 433–436.
- Bulkin, D.A. & Groh, J.M. (2012) Distribution of visual and saccade related information in the monkey inferior colliculus. *Front. Neural. Circuits.*, **6**, 61.
- Buzsáki, G., Anastassiou, C.A. & Koch, C. (2012) The origin of extracellular fields and currents – EEG, ECoG, LFP and spikes. *Nat. Rev. Neurosci.*, **13**, 407–420.
- Coleman, J.R. & Clerici, W.J. (1987) Sources of projections to subdivisions of the inferior colliculus in the rat. *J. Comp. Neurol.*, **262**, 215–226.
- Cooper, A.M. & Cowey, A. (1990) Development and retraction of a crossed retinal projection to the inferior colliculus in neonatal pigmented rats. *Neuroscience*, **35**, 335–344.
- Cooper, M.H. & Young, P.A. (1976) Cortical projections to the inferior colliculus of the cat. *Exp. Neurol.*, **51**, 488–502.
- Covey, E., Hall, W.C. & Kobler, J.B. (1987) Subcortical connections of the superior colliculus in the mustache bat, *Pteronotus parnellii*. *J. Comp. Neurol.*, **263**, 179–197.
- Doubell, T.P., Baron, J., Skalióra, I. & King, A.J. (2000) Topographical projection from the superior colliculus to the nucleus of the brachium of the inferior colliculus in the ferret: convergence of visual and auditory information. *Eur. J. Neurosci.*, **12**, 4290–4308.
- Fisher, N.I. (1993) *Statistical Analysis of Circular Data*. Cambridge University Press, Cambridge.
- Franz, D.N. & Iggo, A. (1968) Conduction failure in myelinated and non-myelinated axons at low temperatures. *J. Physiol.*, **199**, 319–345.
- Freeman, B. & Singer, W. (1983) Direct and indirect visual inputs to superficial layers of cat superior colliculus: a current source-density analysis of electrically evoked potentials. *J. Neurophysiol.*, **49**, 1075–1091.
- Groh, J.M., Trause, A.S., Underhill, A.M., Clark, K.R. & Inati, S. (2001) Eye position influences auditory responses in primate inferior colliculus. *Neuron*, **29**, 509–518.
- Gruters, K.G. & Groh, J.M. (2012) Sounds and beyond: multisensory and other non-auditory signals in the inferior colliculus. *Front. Neural. Circuits.*, **6**, 96.
- Gutfreund, Y., Zheng, W. & Knudsen, E.I. (2002) Gated visual input to the central auditory system. *Science*, **297**, 1556–1559.
- Herbin, M., Repérant, J. & Cooper, H.M. (1994) Visual system of the fossorial mole-lemmings, *Ellobius talpinus* and *Ellobius lutescens*. *J. Comp. Neurol.*, **346**, 253–275.
- Hyde, P. & Knudsen, E. (2002) The optic tectum controls visually guided adaptive plasticity in the owl's auditory space map. *Nature*, **415**, 73–76.
- Itaya, S. & Van Hoesen, G. (1982) Retinal innervation of the inferior colliculus in rat and monkey. *Brain Res.*, **233**, 45–52.
- Jiang, Z.D., Moore, D.R. & King, A.J. (1997) Sources of subcortical projections to the superior colliculus in the ferret. *Brain Res.*, **755**, 279–292.
- Kayser, C., Petkov, C.I. & Logothetis, N.K. (2008) Visual modulation of neurons in auditory cortex. *Cereb. Cortex*, **18**, 1560–1574.
- King, A.J. & Walker, K.M.M. (2012) Integrating information from different senses in the auditory cortex. *Biol. Cybern.*, **106**, 617–625.
- King, A.J., Schnupp, J.W. & Thompson, I.D. (1998) Signals from the superficial layers of the superior colliculus enable the development of the auditory space map in the deeper layers. *J. Neurosci.*, **18**, 9394–9408.
- Lachaux, J.P., Rodriguez, E., Martinerie, J. & Varela, F.J. (1999) Measuring phase synchrony in brain signals. *Hum. Brain Mapp.*, **8**, 194–208.
- Lakatos, P., Chen, C.M., O'Connell, M.N., Mills, A. & Schroeder, C.E. (2007) Neuronal oscillations and multisensory interaction in primary auditory cortex. *Neuron*, **53**, 279–292.
- Lakatos, P., O'Connell, M.N., Barczak, A., Mills, A., Javitt, D.C. & Schroeder, C.E. (2009) The leading sense: supramodal control of neurophysiological context by attention. *Neuron*, **64**, 419–430.

- Makeig, S., Westerfield, M., Jung, T.P., Enghoff, S., Townsend, J., Courchesne, E. & Sejnowski, T.J. (2002) Dynamic brain sources of visual evoked responses. *Science*, **295**, 690–694.
- Manger, P.R., Restrepo, C.E. & Innocenti, G.M. (2010) The superior colliculus of the ferret: cortical afferents and efferent connections to dorsal thalamus. *Brain Res.*, **1353**, 74–85.
- Mascetti, G.G. & Strozzi, L. (1988) Visual cells in the inferior colliculus of the cat. *Brain Res.*, **442**, 387–390.
- Musacchia, G. & Schroeder, C.E. (2009) Neuronal mechanisms, response dynamics and perceptual functions of multisensory interactions in auditory cortex. *Hearing Res.*, **258**, 72–79.
- Naue, N., Rach, S., Strüber, D., Huster, R.J., Zaehle, T., Körner, U. & Herrmann, C.S. (2011) Auditory event-related response in visual cortex modulates subsequent visual responses in humans. *J. Neurosci.*, **31**, 7729–7736.
- Nolte, G., Bai, O., Wheaton, L., Mari, Z., Vorbach, S. & Hallett, M. (2004) Identifying true brain interaction from EEG data using the imaginary part of coherency. *Clin. Neurophysiol.*, **115**, 2292–2307.
- Nolte, G., Ziehe, A., Nikulin, V., Schlögl, A., Krämer, N., Brismar, T. & Müller, K.-R. (2008) Robustly estimating the flow direction of information in complex physical systems. *Phys. Rev. Lett.*, **100**, 234101.
- Populin, L.C. & Yin, T.C.T. (2002) Bimodal interactions in the superior colliculus of the behaving cat. *J. Neurosci.*, **22**, 2826–2834.
- Porter, K.K., Metzger, R.R. & Groh, J.M. (2006) Representation of eye position in primate inferior colliculus. *J. Neurophysiol.*, **95**, 1826–1842.
- Porter, K., Metzger, R. & Groh, J. (2007) Visual- and saccade-related signals in the primate inferior colliculus. *Proc. Natl. Acad. Sci. USA*, **104**, 1826–1842.
- Schroeder, C.E. & Foxe, J. (2005) Multisensory contributions to low-level, ‘unisensory’ processing. *Curr. Opin. Neurobiol.*, **15**, 454–458.
- Sieben, K., Röder, B. & Hanganu-Opatz, I.L. (2013) Oscillatory entrainment of primary somatosensory cortex encodes visual control of tactile processing. *J. Neurosci.*, **33**, 5736–5749.
- Stein, B.E. & Meredith, M.A. (1993) *The Merging of the Senses*. The MIT Press, Cambridge, MA.
- Stein, B.E. & Wallace, M.T. (1996) Comparisons of cross-modality integration in midbrain and cortex. *Prog. Brain Res.*, **112**, 289–299.
- Stütt, I., Galindo-Leon, E., Pieper, F., Engler, G. & Engel, A.K. (2013) Laminar profile of visual response properties in ferret superior colliculus. *J. Neurophysiol.*, **110**, 1333–1345.
- Tawil, R.N., Saadé, N.E., Bitar, M. & Jabbur, S.J. (1983) Polysensory interactions on single neurons of cat inferior colliculus. *Brain Res.*, **269**, 149–152.
- Waleszczyk, W.J., Wang, C., Benedek, G., Burke, W. & Dreher, B. (2004) Motion sensitivity in cat’s superior colliculus: contribution of different visual processing channels to response properties of collicular neurons. *Acta Neurobiol. Exp.*, **64**, 209–228.
- Wallace, M.T., Wilkinson, L.K. & Stein, B.E. (1996) Representation and integration of multiple superior colliculus sensory inputs in primate. *J. Neurophysiol.*, **76**, 1246–1266.
- Yamauchi, K. & Yamadori, T. (1982) Retinal projection to the inferior colliculus in the rat. *Acta Anat.*, **114**, 355–360.
- Zwiers, M.P., Versnel, H. & Van Opstal, A.J. (2004) Involvement of monkey inferior colliculus in spatial hearing. *J. Neurosci.*, **24**, 4145–4156.